Master's Thesis of Engineering

Dimensionality-Dependent Plasticity in Halide Perovskite Artificial Synapses for Neuromorphic Computing

뉴로모픽 컴퓨팅을 위한 할라이드 페로브스카이트 인공시냅스의 차원에 따른 시냅틱 거동

February 2019

Graduate School of Engineering
Seoul National University
Department of Materials Science and Engineering

Sung-Il Kim

Dimensionality-Dependent Plasticity in Halide Perovskite Artificial Synapses for Neuromorphic Computing

Tae-Woo Lee

Submitting a master's thesis of Public Administration

February 2019

Graduate School of Engineering
Seoul National University
Department of Materials Science and Engineering

Sung-Il Kim

Confirming the master's thesis written by
Sung-Il Kim
February 2019

Chair	Ho Won Jang	(Seal)
Vice Chair	Tae-Woo Lee	(Seal)
Examiner	Jin Young Kim	(Seal)

Abstract

Dimensionality-Dependent Plasticity in Halide Perovskite Artificial Synapses for Neuromorphic Computing

Kim, Sung-Il
Department of Materials Science and Engineering
Seoul National University

Organic-inorganic halide perovskites (OHPs) have unique hysteresis behavior caused by ion migration, so they may have applications as the active material of artificial synapses for neuromorphic electronics, which mimic structures and functions of biological neurons and synapses. Here we demonstrate artificial synapses with two-dimensional (2D) and Quasi-2D perovskite that have a layer of bulky organic cation (phenethylammonium (PEA)) to form structures of $(PEA)_2MA_{n-1}Pb_nBr_{3n+1}$. The OHP films have morphological properties that depend on the structure dimensionality, and OHP artificial synapses show synaptic responses such as short-term plasticity, paired-pulse facilitation, and long-term plasticity. We also analyzed the operation mechanism of OHP artificial synapses and Quasi-2D (n = 3, 4, 5) OHP artificial synapses showed much longer retention time compared with 2D and 3D OHP counterparts. The calculated energy consumption of 2D OHP artificial synapse (~0.7 fJ/synaptic event) was comparable to that of the biological synapse (1-10 fJ/synaptic event). These OHP artificial synapses may enable development of neuromorphic electronics based on OHP artificial synapses.

Keyword : neuromorphic memory, perovskite memristors, artificial synapses, Quasi-2D perovskite, perovskite synapses
Student Number : 2017-21688

Table of Contents

List of Figures

List of Tables

Chapter 1. Introduction

Human brain controls most movements and homeostasis such as heartbeat, the blood pressure, and the body temperature and performs cognition, memory, and learning with low power consumption (~20 W) based on three-dimensional (3D) neural network consisted of 100 billion neurons and 100 trillion synapses.[1,2] Conventional von Neumann computing architecture sequentially processes data and it is excellent for numerical calculation. However, for development of future artificial intelligence, the conventional system has limitations to conduct deep learning such as pattern recognition, real-time information processing, and decision making, because it requires huge hardware architectures and extremely high power consumption (~1.4 MW) due to the von Neumann bottleneck.[3]

Neuromorphic computing emulates the functions of a brain and operates at low power, so it is becoming a core technology to demonstrate future artificial intelligence and to overcome the limitations of conventional structures, such as huge hardware architectures and high power consumption. To implement the neuromorphic system, various types of electronic devices have been developed based on phase-change memory,[4] resistive switching memory,[5] magnetoresistive memory,[6] atomic switches,[7] and synaptic functional transistors.[8,9] Although these devices could mimic the important properties of biological synapses and perform parallel operations, they require larger energy than a biological synapse. Therefore, development of an artificial synapse with energy consumption on the level of a biological synapse remains an open problem. Organic-inorganic halide perovskite (OHPs) have been evaluated as a technology to solve it.

OHPs have an ABX_3 crystal structure; the A-site cation is located at the center of a BX_6 octahedral cage, and the B-site metal cation is surrounded by the six nearest-neighbor X-site halide anions.[10]

OHPs have a significant hysteresis property that is caused by ion migration or space charges, or both, which may enable memory properties based on OHP.[11]

Two-terminal artificial synapses based on 3D methylammonium (MA) lead halide perovskite ($MAPbX_3$, X = Br, I) films show synaptic responses that are caused by ion migration in the OHP layer.[12,13] Ion migration in 3D OHP film is induced by relatively low energy, but it can be further reduced to the energy level of biological synapses by engineering the structure of OHP films.

In this work, we introduce two-dimensional (2D) and Quasi-2D OHP films into artificial synapses, to enable control of ion migration and resultant synaptic responses. For this purpose, were placed the small MA ion with a bulky phenethylammonium (PEA) ion in their crystalline structures. To prepare 2D, Quasi-2D, and 3D OHP films, we controlled the stoichiometric ratio of PEA and MA cations to induce self-assembly of a layered structure. This replacement of an MA cation with PEA cation suppresses ion migration in the out-of-plane direction of the OHP films.[14-16] Thereby, the activation energy E_A of ion migration is increased, so ion migration and excitatory post-synaptic current (EPSC) can be reduced. Also, energy consumption of the device is reduced to ~0.7 fJ/synaptic event, which is comparable to the consumption of biological synapses. Memory retention of artificial synapse was controlled by adjusting the dimensionality of the perovskite structure. We quantified synaptic properties such as paired-pulse facilitation (PPF), short-term potentiation (STP), long-term potentiation (LTP), spike-frequency dependent plasticity (SFDP), spike-duration dependent plasticity (SDDP), spike-voltage dependent plasticity (SVDP), and spike-number dependent plasticity (SNDP). This OHP artificial synapse that uses low power may facilitate realization of energy-efficient neuromorphic systems.

Chapter 2. Experimental

2.1. Perovskite solution preparation

Lead bromide ($PbBr_2$, 99.999%, Sigma-Aldrich), phen-ethylammonium bromide (PEABr, Greatcell Solar Korea), and methylammoniumbromide (MABr, Great cell Solar Korea) were dissolved in dimethylsulfoxide (DMSO, >99.9%, Sigma-Aldrich).

2.2. Device fabrication

ITO-coated glass (AMG) was cleaned by sonication in acetone and 2-propanol. BCCP composed of poly(3,4-ethylene dioxythiophene)-poly(styrene sulfonate) (PEDOT:PSS) (Heraeus CleviosTM AI 4083) with a perfluorinated ionomer (PFI), tetrafluoroethylene-perfluoro-3,6-dioxa-4-methyl-7-octenesulfonic acid copolymer (PEDOT:PSS:PFI = 1:2.5:11.2 (w:w:w)) was spin-coated on cleaned ITO substrates at a speed of 4500 rpm, then baked at 150 ℃ for 30 min. $(PEA)_2(MA)_{n-1}Pb_nBr_{3n+1}$ solution was then spin-coated on the BCCP thin layer at 3000 rpm for ~80 s in a nitrogen-filled glove box with nanocrystal-pinning (NCP) process by using anti-solvent (toluene) at room temperature, followed by thermal annealing at 90 ℃ for 10 min. Then 100-nm-thick Al layer thermally evaporated as a top electrode using a metal shadow mask in a high-vacuum chamber ($<10^{-6}$ Torr). The device area is 0.0625 mm^2.

2.3. Measurements

Scanning electron microscopy (SEM) imaging was gained by a SUPRA 55VP field-emission microscope. PL measurement of OHP

films were measured using a JASCO FP8500 spectrofluorometer. The X-ray diffraction (XRD) measurements were performed by an X-ray diffractometer (BRUKER MILLER Co., D8-Advance) with Cu Kα radiation (λ = 1.54056 Å). XRD data were gained in the 2θ range of 8° -50° at room temperature. The electric characteristics of the electronic devices were mostly measured in a nitrogen-filled glove box by using a Keysight B1500 semiconductor parameter analyzer to apply scanning bias and perform the output current. The pulse mode function of Keysight B1500 was used for the pulse mode measurement. To obtain the resistance of the flims, the devices were measured using and Agilent 4156C semiconductor analyzer in the current voltage sweeping mode in a vacuum chamber (6×10^{-6} Torr).

Chapter 3. Results and Discussion

3.1. Structure of halide perovskite artificial synapses and perovskites

The OHP artificial synapses were fabricated with the two-terminal device structure of ITO (bottom electrode)/buffer-capped conducting polymer (BCCP)/OHP/Al (top electrode) (**Figure 3.1**), where BCCP consists of poly(3,4-ethylenedioxythiophene)-poly(styrene sulfonate) (PEDOT:PSS) (Heraeus Clevios™ AI 4083) with a perfluorinated ionomer (PFI), tetrafluoro ethylene-perfluoro-3,6-dioxa-4-methyl-7- octenesulfonic acid copolymer (PEDOT:PSS:PFI = 1:2.5:11.2 (w:w:w)). The Al top electrode mimics the pre-synaptic membrane to which the pre-synaptic spike is applied, and the ITO bottom electrode mimics the post-synaptic membrane at which the post-synaptic current is read. A synaptic electrical spike applied to the top electrode induces ion migration and consequently modulates the conductance of the OHP thin films.[12] The BCCP layer blocks the formation of conductive filaments through the devices, so the devices do not have bi-stable states.

OHP films with 2D, Quasi-2D, and 3D structures were used as the active layers of artificial synapses. The configuration of OHP thin films could be defined by the number of $PbBr_6$ layers between PEA layers; this number depends on the ratio of MA and PEA cations, and the molecular formula of OHPs can be expressed as $(PEA)_2MA_{n-1}Pb_nBr_{3n+1}$. The structural dimensionality depends on the ratio.[17] For example, if n = 1, one $PbBr_6$ layer forms between the large organic ammonium layers, so 2D $(PEA)_2PbBr_4$ is achieved; if $n \geq 2$, two or a few $PbBr_6$ layers form between the large organic ammonium layers, so Quasi-2D $(PEA)_2MA_{n-1}Pb_nBr_{3n+1}$ forms; and if $n = \infty$, 3D $MAPbBr_3$ forms (**Figure 3.2**).

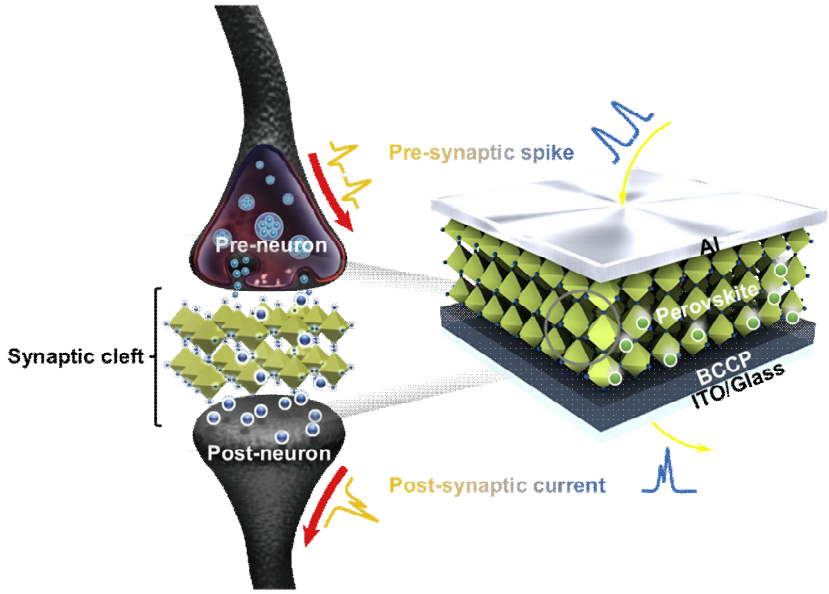

Figure 3.1 Structure of perovskite artificial synapses

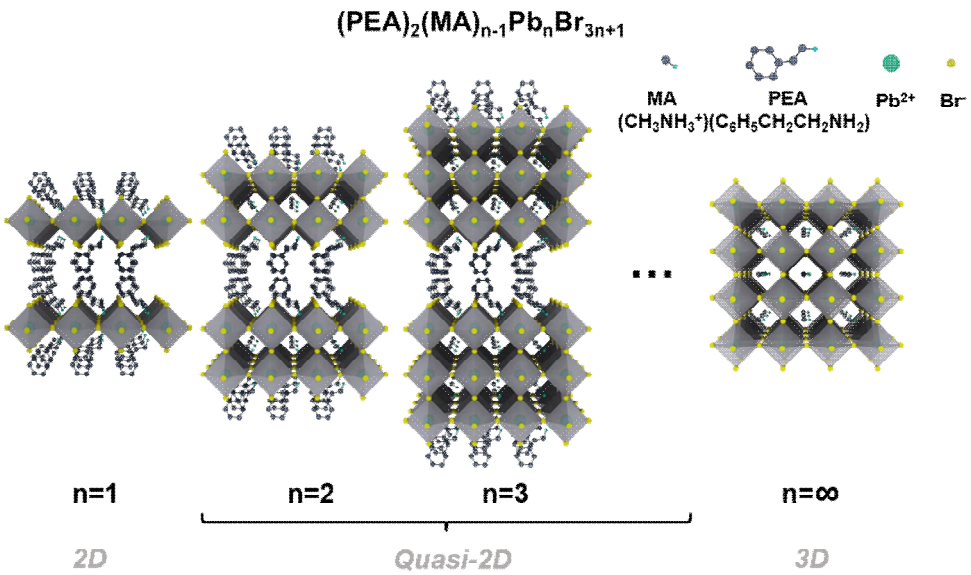

Figure 3.2 Crystal structure of perovskite with structural dimensionality Structure of perovskite artificial synapses

3.2. Optical Analysis of perovskite films

$(PEA)_2MA_{n-1}Pb_nBr_{3n+1}$ (n = 1–5, ∞) films were spin–coated on BCCP/ITO substrate in an N_2–filled glovebox. Toluene was used as an anti–solvent for the nanocrystal–pinning (NCP) process (**Figures 3.3**), so the thin–films were pinhole–free with smooth surfaces (**Figures 3.4, 3.5**). As n increased, the bandgap of OHPs decreased,[14,17] so the films became yellowish. The films showed different photoluminescence (PL) under UV (365 nm) lamp excitation (**Figures 3.6**). 2D $(PEA)_2PbBr_4$ (n = 1) emitted blue PL because of the strong quantum confinement in a very thin quantum well. Quasi–2D ($2 \leq n \leq 5$) films emitted bright greenish PL due to energy funneling.[10] 3D $MAPbBr_3$ (n = ∞) showed no PL emission because the excitons have low exciton binding energy at room temperature, so they are dissociated.[14]

In steady–state PL measurement, the structural relaxation of the crystal lattice increased the optical bandgap, so the lattice expansion in 2D $(PEA)_2PbBr_4$ film yielded a blue–shifted PL spectrum (**Figures 3.7**, and **Table 3.1**).[18] In UV–vis absorption spectra, 2D $(PEA)_2PbBr_4$ and 3D $MAPbBr_3$ films showed absorption peaks near wavelengths λ = 401 nm and 525 nm, respectively. In contrast, the absorption peaks of Quasi–2D perovskite films gradually red–shifted to λ = 401, 432, 450 nm ($2 \leq n \leq 5$) as n increased because of different quantum and dielectric confinement effects;[10,14] and the absorption peaks at 401 nm and 432 nm became strong because proportions of n = 1, 2 domains became dominant.[14,19]

The X–ray diffraction (XRD) patterns of the films showed a clear tendency of structural changes from 2D to 3D as n increased (**Figures 3.8**).[14] For 2D $(PEA)_2PbBr_4$ (n = 1), (00l) reflections were dominant; this result is characteristic of an ordered layer structure in the out–of–plane direction of the 2D layers.[18] Quasi–2D perovskite films ($2 \leq n \leq 5$) showed additional peaks depending on the number of layers. For 3D $MAPbBr_3$ (n = ∞),

(h00) reflections were dominant.

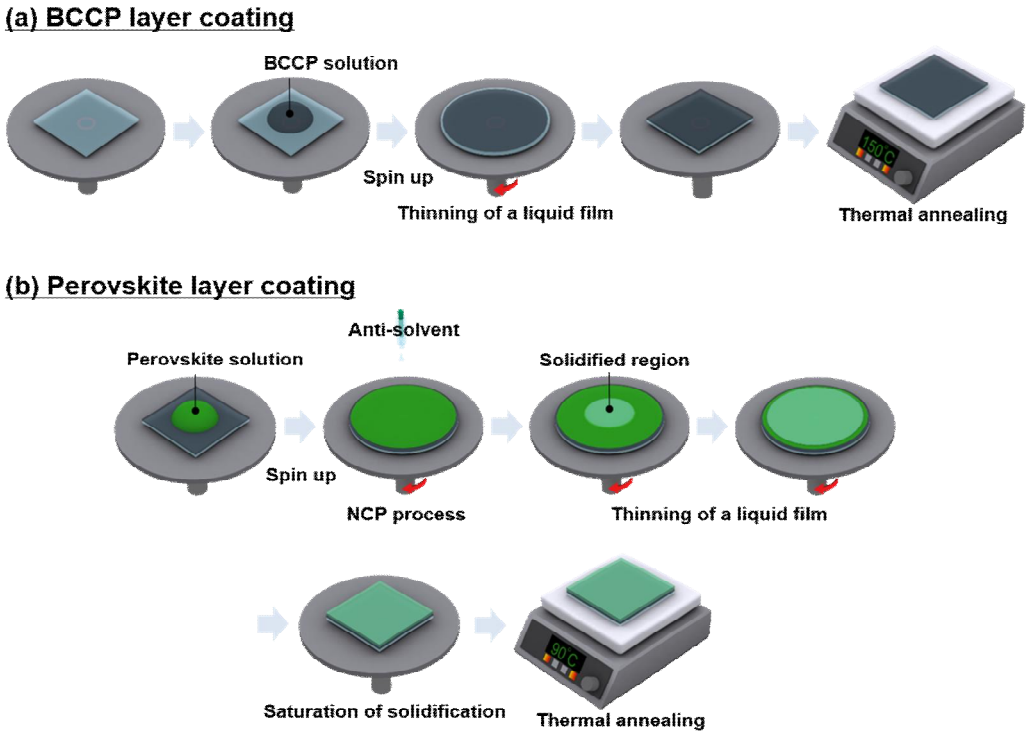

Figure 3.3 The fabrication process of perovskite artificial synapse

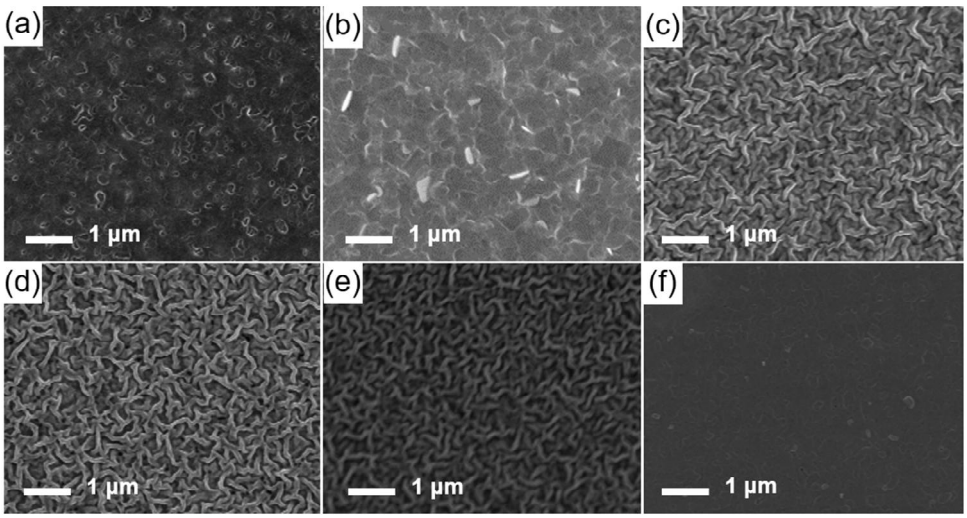

Figure 3.4 SEM images of morphology of perovskite thin-films

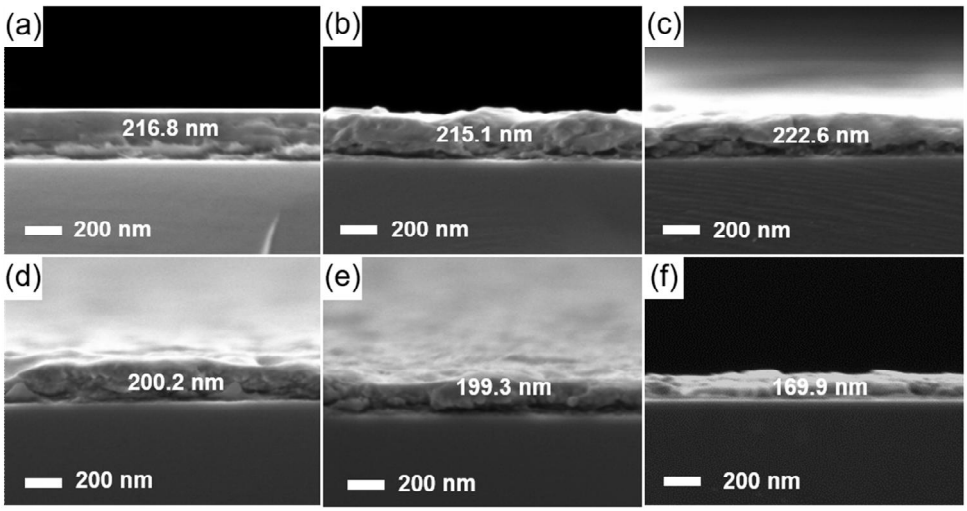

Figure 3.5 SEM images of cross-sectional images of perovskite thin-films

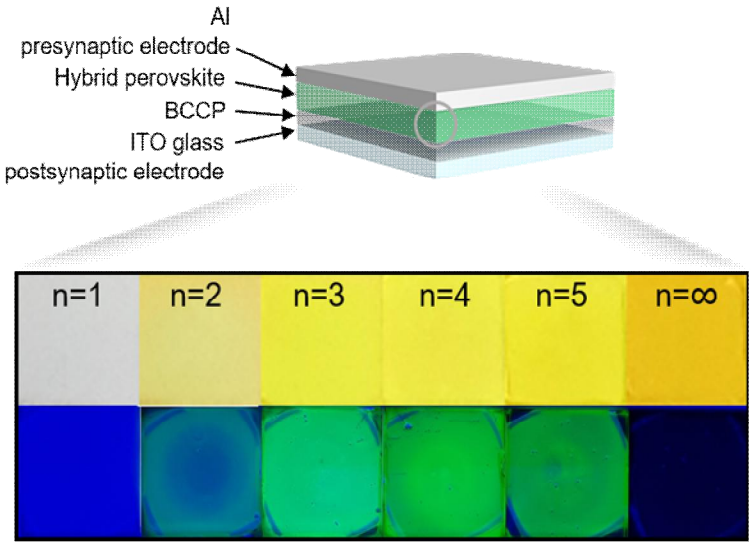

Figure 3.6 Film images of perovskite thin-film under light (top) and their luminescence when UV (365 nm) was irradiated (bottom).

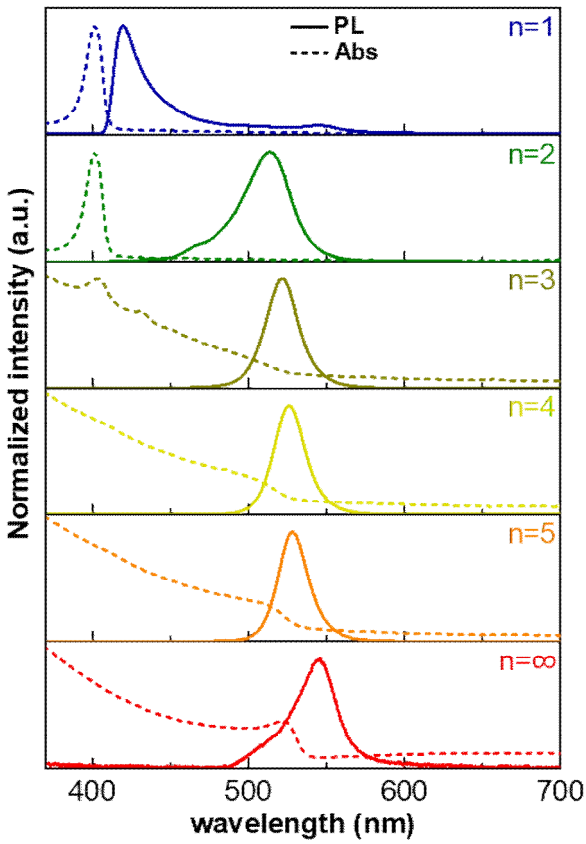

Figure 3.7 UV-Vis absorption and photoluminescence (PL) spectra

Configuration	Thickness (nm)	Peak wavelength (nm)
$n = 1$	216.8	419.5
$n = 2$	215.1	513.5
$n = 3$	222.6	521.8
$n = 4$	200.2	526.2
$n = 5$	199.3	528.4
$n = \infty$	169.9	545.9

Table 3.1 The thickness and peak wavelength of PL spectra of perovskite films

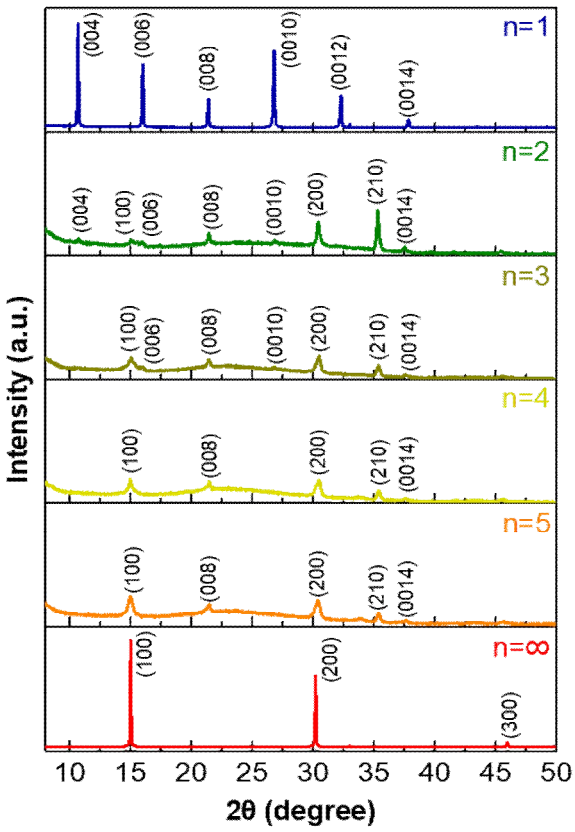

Figure 3.7 XRD spectra of $(PEA)_2MA_{n-1}Pb_nBr_{3n+1}$

3.3. Spike-dependent plasticity in artificial synapses

Synaptic plasticity is involved in learning and memory by strengthening or weakening synaptic weight over time in response to synaptic activity.[20] In a biological synapse, excitatory post-synaptic response shows a temporary increase in synaptic weight due to the flow of ions at the post-synaptic membrane. Similarly, in our device, when pulse was applied temporarily, the post-synaptic current was abruptly increased by voltage-induced ion migration, then gradually decayed over time due to back-diffusion of ions (**Figure 3.9**). In Quasi-2D perovskites, the large insulating PEA cations suppress charge transport so the conductivity decreases as the ratio of PEA increases, i.e., as n decreases.[14]

In a biological synapse, STP is a temporal modulation of synaptic strength; it is involved in pattern recognition, associative learning, and sound localization.[3,21] If stimuli are not sustained, the post-synaptic current quickly returns to the initial state within hundreds to thousands of milliseconds. In our artificial synapse, when negative pre-synaptic voltage pulses (−1 V) were applied, EPSC was induced by migration of bromide ions (Br^-), and yielded a temporary enhancement of the conductivity of OHP. After the voltage pulses are removed, migrated ions diffused back to the original position, so the film conductivity decreased and current is decayed.

PPF is a kind of STP in which the synaptic strength temporarily increases when paired-pulses are applied within a short interval Δt. Analogously, the synaptic weight of our artificial synapse increased when two consecutive stimuli were applied (**Figure 3.10**). The change in conductance of the OHP layer was dependent on Δt. PPF increased as Δt decreased from 180 to 20 ms, because back-diffusion of Br^- ions decreased as Δt was decreased; therefore, learning and memory are strengthened.

SFDP is considered to be an extended form of Hebbian learning, and is related to learning, associative memory, and forgetting.[22]

Repeated synaptic spikes with various frequency (2.8 to 25 Hz) were applied to the artificial synapse (**Figure 3.11**). EPSC increased as the spike frequency increased, because high-rate pulses increased ion migration and prevented back-diffusion of ions in the OHP when the pulse was removed.

SVDP, SDDP, and SNDP were also observed in our artificial synapse (**Figure 3.12-3.17**).[23] As the pulse magnitude (from 0.1 to 1.8V), the pulse duration (from 20 to 200 ms), and the number of pulses (from 1 to 50) were increased, the number of Br^- that migrated increased and the induced changes in conductivity of OHP increased, so EPSC increased proportionally.

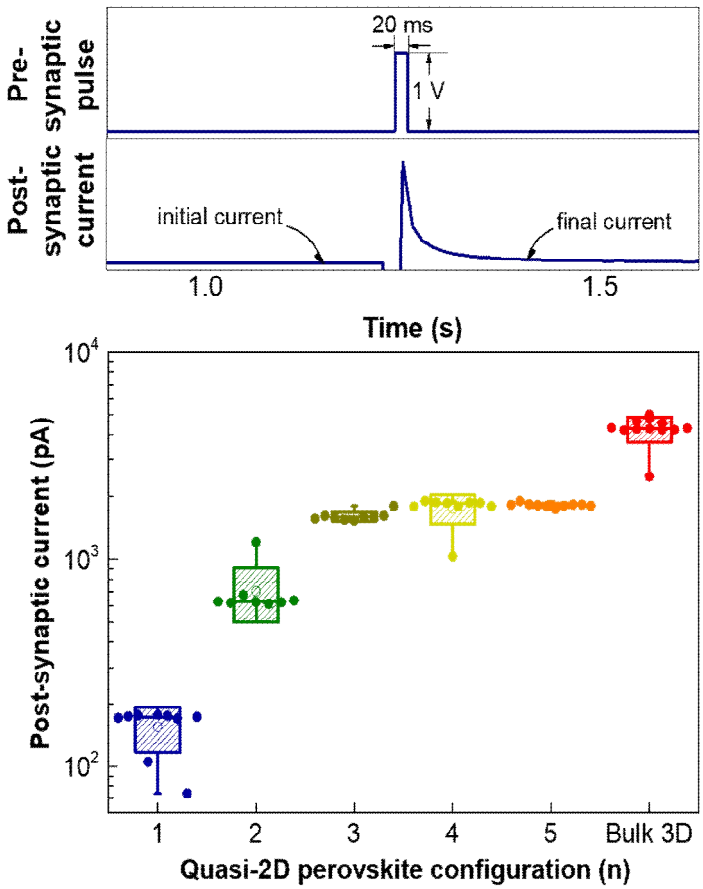

Figure 3.9 Excitatory post-synaptic current (EPSC) of perovskite artificial synapse triggered by an applied external pulse

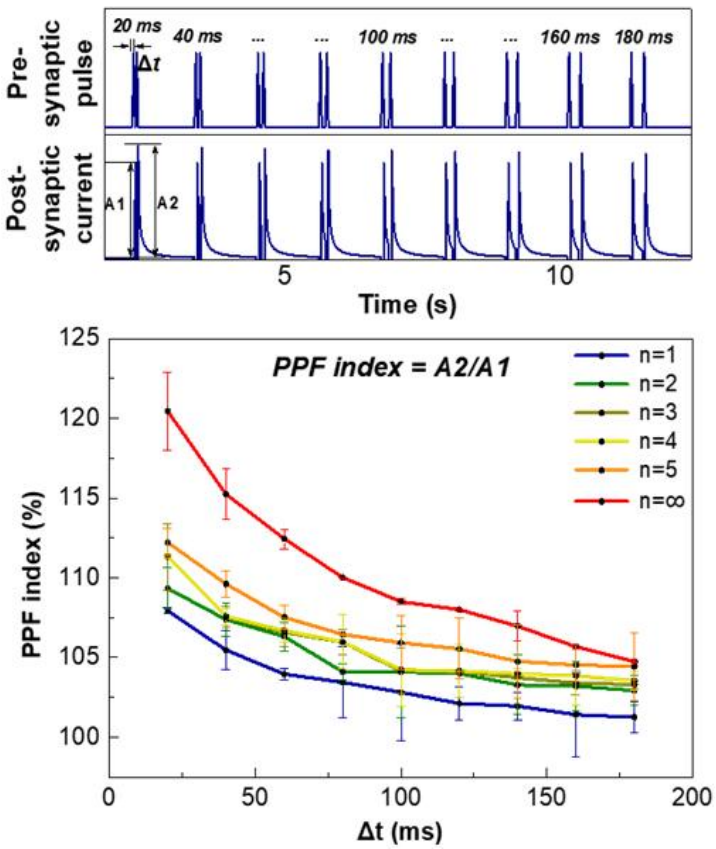

Figure 3.10 Paired pulse facilitation (PPF) index (A2/A1) achieved by two successive pulses with various time interval

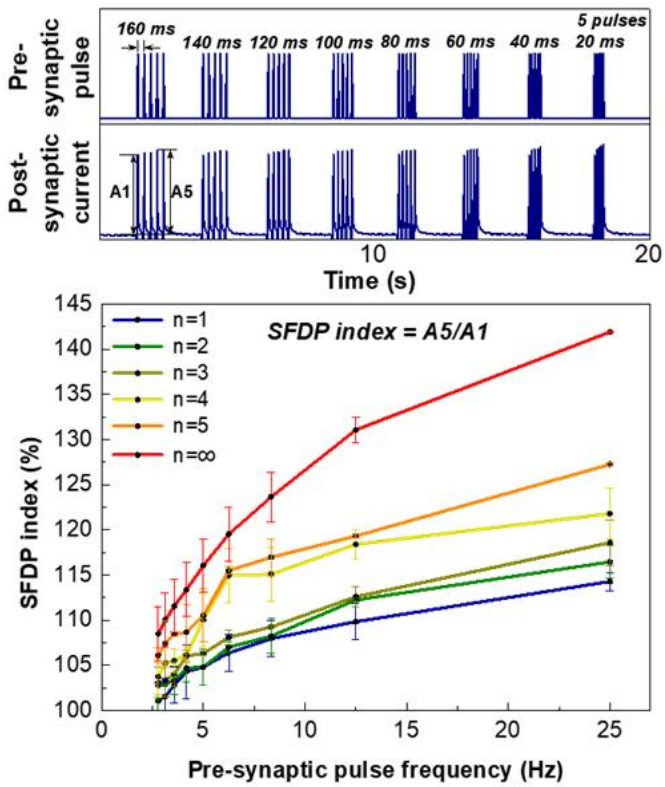

Figure 3.11 SFDP index (A5/A1) according to the spike frequency

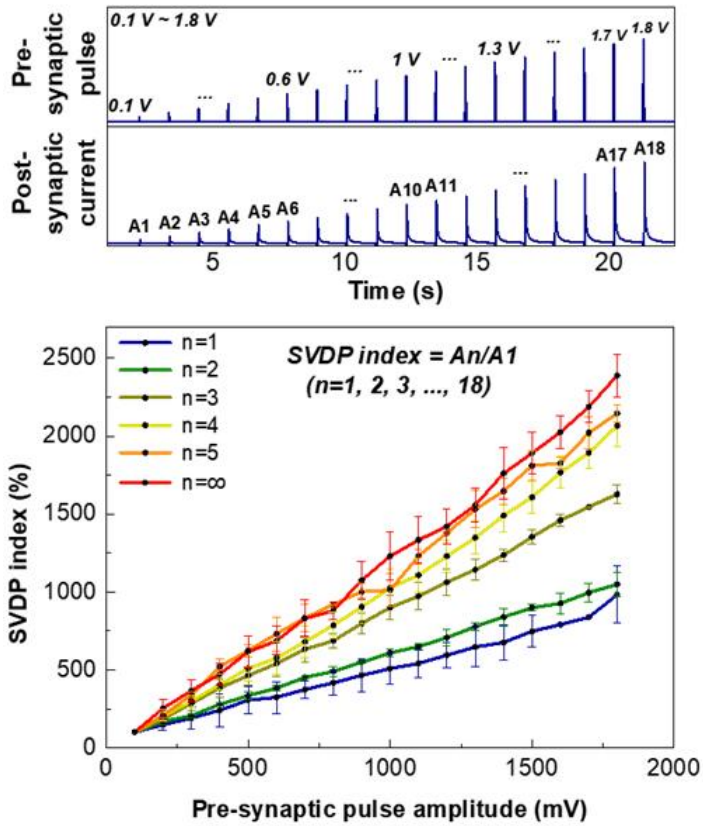

Figure 3.12 SVDP index (A*n*/A1) according to the spike voltage amplitude

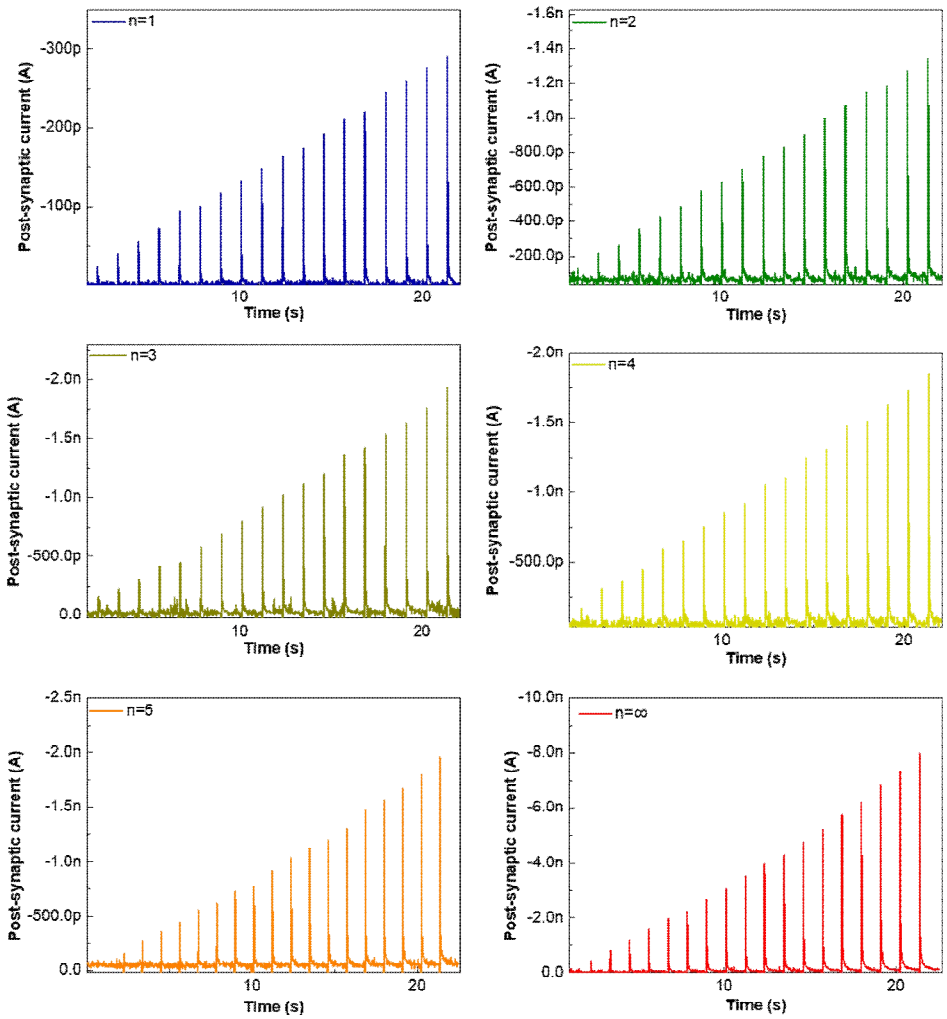

Figure 3.13 Spike-voltage dependent plasticity (SVDP) in perovskite artificial synapse

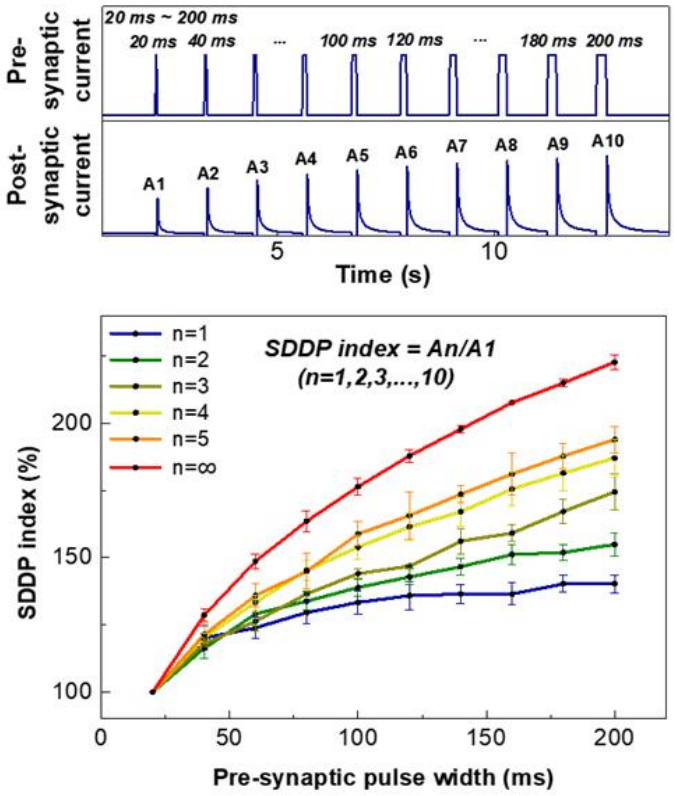

Figure 3.14 Spike-duration dependent plasticity (SDDP) index (A*n*/A1) according to the spike duration

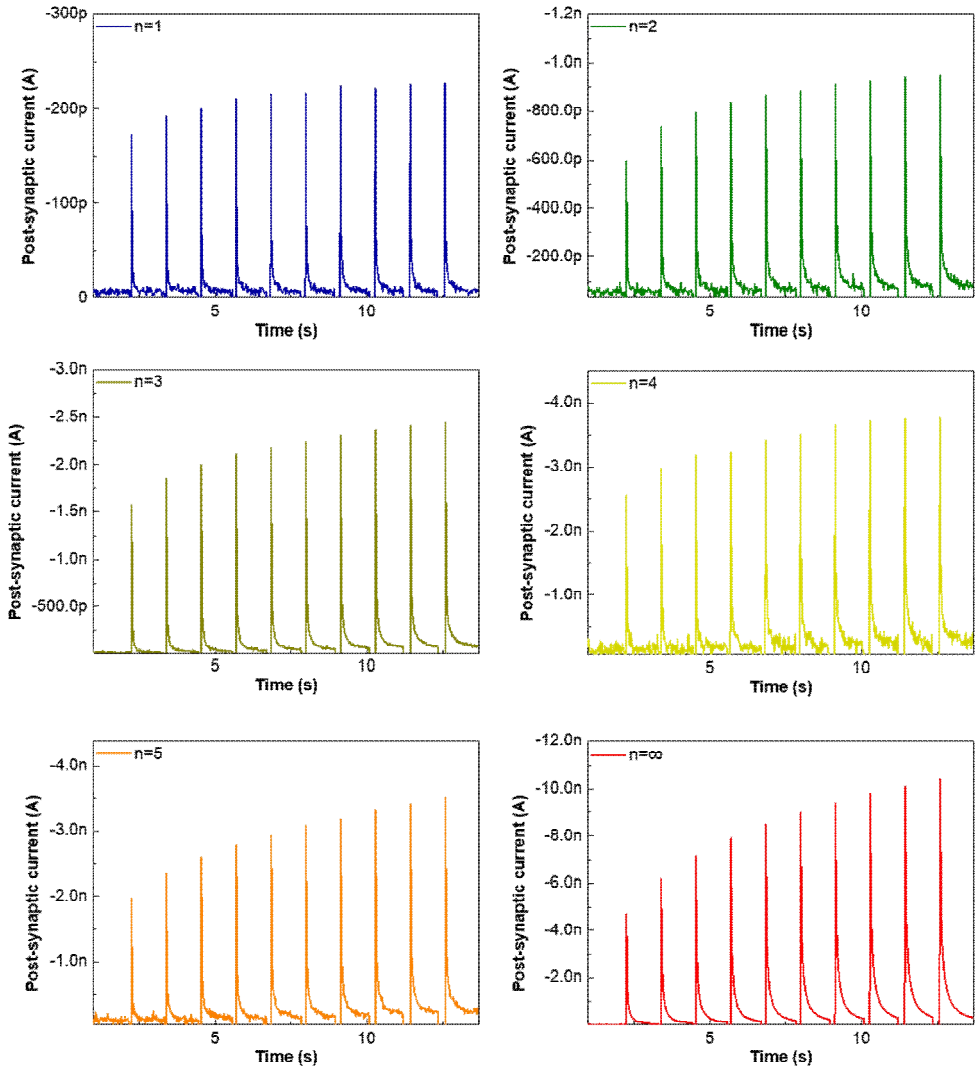

Figure 3.15 SDDP in perovskite artificial synapse

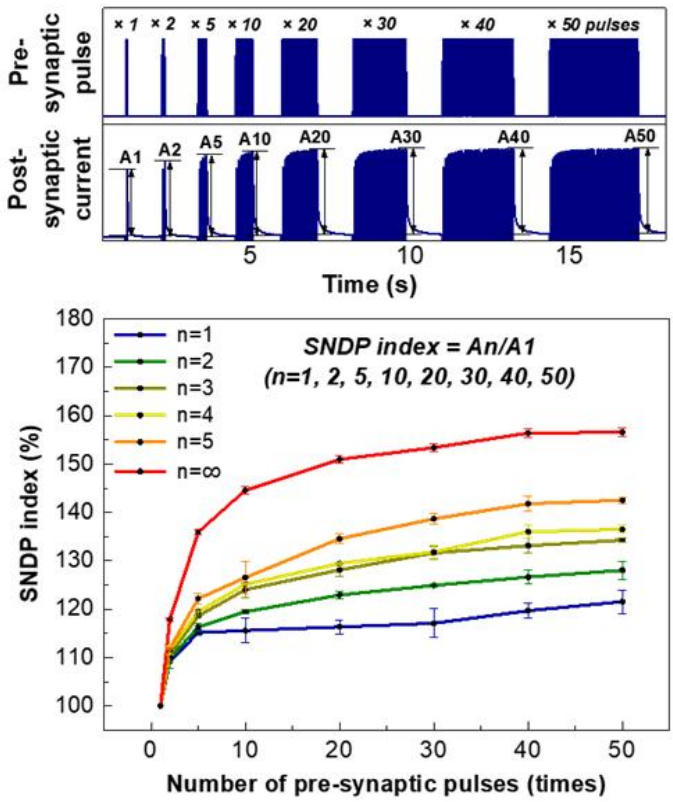

Figure 3.16 Spike-number dependent plasticity (SNDP) index (A*n*/A1) according to the number of spikes amplitude

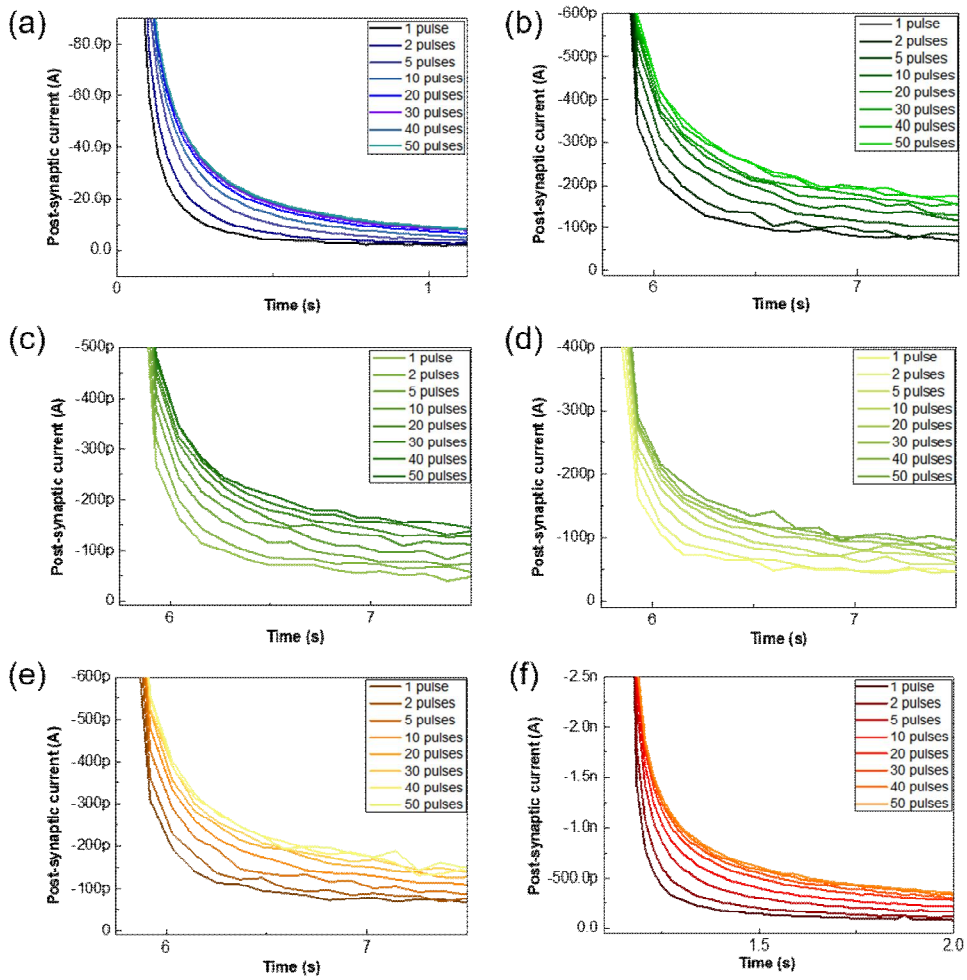

Figure 3.17 SNDP in perovskite artificial synapses with structural dimensionality from 1 to ∞. (a) PEA_2PbBr_4 (n = 1), (b) $PEA_2MAPb_2Br_7$ (n = 2), (c) $PEA_2MA_2Pb_3Br_{10}$ (n = 3), (d) $PEA_2MA_3Pb_4Br_{13}$ (n = 4), (e) $PEA_2MA_4Pb_5Br_{16}$ (n = 5), and (f) $MAPbBr_3$ (n = ∞). Pulses had magnitude of 1 V and duration of 20 ms. The magnitude of read voltage was 0.01 V.

3.4. Long-term plasticity (LTP) in artificial synapses

The multi-store model proposed by Atkinson and Shiffrin suggests that human memory has three components: sensory memory, short-term memory and long-term memory (**Figure 3.18**).[23] If sensory stimuli are repeated frequently, short-term memory is converted to long-term memory. Similarly, we can induce the STP-LTP transition in our artificial synapses by applying several repeated stimuli (**Figure 3.19**). The memory decay curve in our artificial synapse is similar to the 'forgetting curve' (**Figure 3.17**).[23] When 30 pulses were applied, the decay of memory retention fitted a power function $y = b \times t^{-m}$, where y is the synaptic weight, b is the fit constant for scaling, t is the time, and m is the power function rate.[22] As m decreases, the retention curve decreases; i.e., the duration of memory increases. Quasi-2D films with n = 3, 4, 5 have smaller m than 3D film, so Quasi-2D films have longer retention time than 3D film. The difference occurs because back-diffusion of migrated anions is hindered by the bulky PEA cations when the voltage is removed, so the increased current is maintained for a long time. However, in Quasi-2D films with n = 1, 2, the large content of insulating PEA would allow only a few ions to migrate when the voltage is applied, so it seems that the potentiated current retention is unnoticeable.

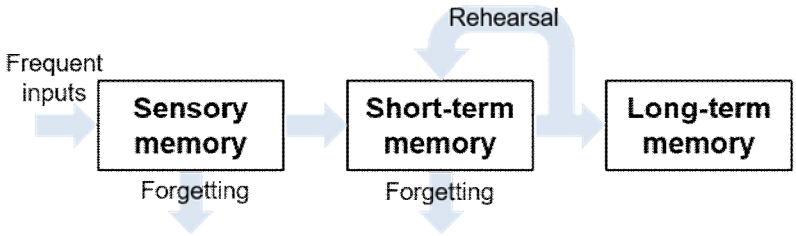

Figure 3.18 Schematic demonstrations of the multi-store model of human memory proposed by Atkinson and Shiffrin

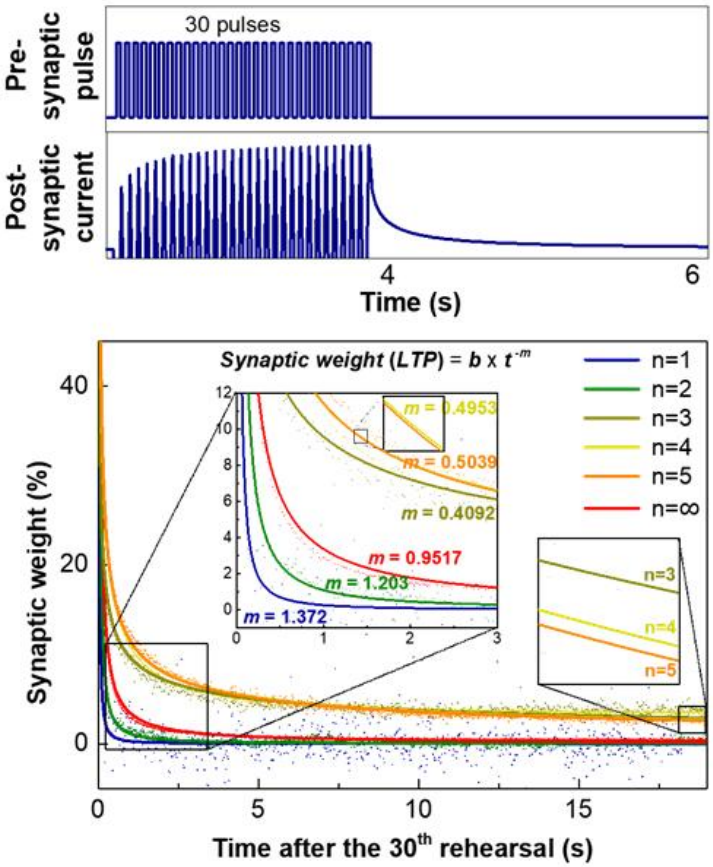

Figure 3.19 Current decay curves of perovskite synapses

3.5. Ion migration in artificial synapses

We hypothesize that the dimensionality of the OHP film affects the migration of ions in it. When voltage pulses are applied, ions migrate, and then when the voltage pulses are removed, the ions diffuse back into their original distribution.[12] In 3D films, ions are relatively free to move along defects such as grain boundaries (**Figure 3.20**).[24] In contrast, in Quasi-2D perovskites, the large insulating PEA cationsare distributed at $PbBr_6$ layers boundaries because PEA cations structurally cover the $PbBr_6$ layers (**Figure 3.20**), so the PEA ions impede movement of halide ions and thereby increase the E_A of halide ion migration.[25] Therefore, as the amount of PEA increases (e.g., n = 1, 2), the migration of Br^- ions is significantly suppressed. As n of Quasi-2D perovskites increases (n = 3, 4, 5), the ease of Br^- ion migration increases compared to low-dimensional Quasi-2D (n = 1, 2) when driving voltage is applied, but when the voltage is removed, the PEA impedes ion back-diffusion in Quasi-2D perovskites.

We compared E_A in all OHP films to support our explanation (**Figure 3.21**). Br^- ions have the smallest E_A in the 3D $MAPbBr_3$ film (**Table 3.2**),[26-28] so when applied voltage is small (-1 V), most of the ions that migrate in the OHP films may be Br^-.[12] In Arrhenius plots of OHP films by the equation of $\ln R(T) = \ln R_0 + E_A/kT$, where R is the resistance, R_0 is the constant, k is the Boltzmann constant, and T is the absolute temperature. The magnitude of E_A decreased as n increased (**Table 3.3**). Under the bias, Br^- ions and MA^+ ions may be accumulated at the anode and cathode side, respectively; these induce band bending at the interface and facilitate charge injection into OHP films. As PEA concentration increased, ion migration is suppressed due to bulky PEA, and thus ion accumulation is prevented. This behavior can be confirmed by the resistance change of OHP film, which is influenced by the increase in charge injection barrier. Thus, from the temperature-dependent conductance by the flow of charge carriers, we could

infer the degree of ion migration. Therefore, Quasi-2D OHPs which had higher activation energy of ion migration and charge accumulation might show the less increased conductance (i.e. high resistance) with increasing temperature. In other words, we deduce that PEA in Quasi-2D OHP films has a major effect on activation of ion transport and on back-diffusion of ions in OHP layers, and consequently can control synaptic plasticity of perovskite synapses.

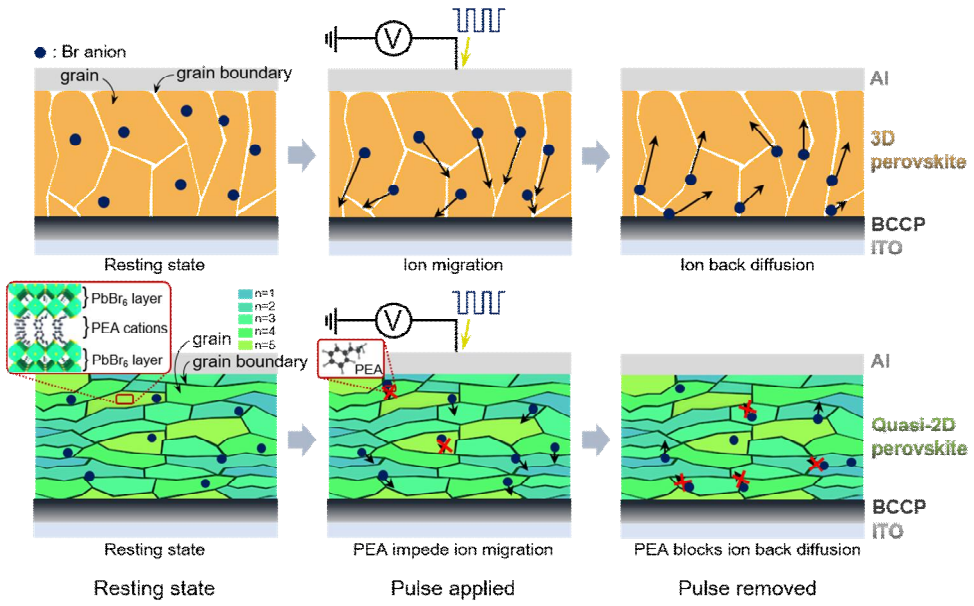

Figure 3.20 Schematics of ion migration in the 3D and Quasi-2D perovskite layers

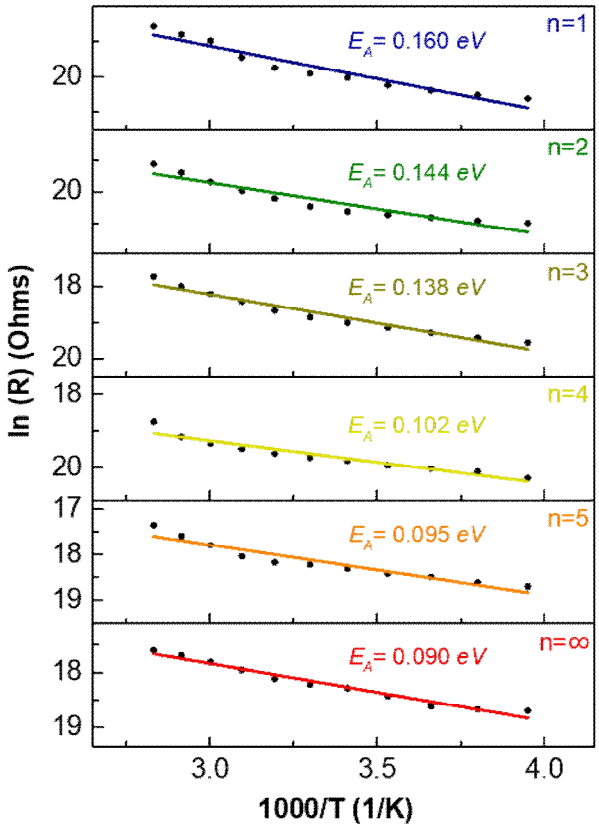

Figure 3.20 The Arrhenius plot of resistance in perovskite artificial synapse

Defect	Defect notation	E_A (eV)
$CH3NH3^+$ (MA^+)	V'_{MA}	0.46-0.56 [26]
		0.84 [27]
		0.80-1.13 [28]
Pb^{2+}	V''_{Pb}	0.80 [26]
		2.31 [27]
		1.35-1.80 [28]
Br^-	$V^{\bullet}_{Br}$	0.09-0.16 [26]
		0.2-0.46 [28]

Table 3.2 The constant of the memory retention curve and activation energies for ion vacancy migration in halide perovskite artificial synapse

Configuration	Fit constant (*b*)	Power function rate (*m*)	E_A (eV)
***n* = 1**	0.002795	1.372	0.160
***n* = 2**	0.01096	1.205	0.144
***n* = 3**	0.09594	0.4092	0.138
***n* = 4**	0.1142	0.4953	0.102
***n* = 5**	0.1145	0.5039	0.095
***n* = ∞**	0.03129	0.9517	0.090

Table 3.3 Summary of device structures and energy consumption of artificial synaptic devices

3.6. Energy efficiency of artificial synapses

A biological synapse has high energy efficiency (1−10 fJ per synaptic event).[22] The energy consumption of the artificial synapse is calculated as $E = PIt$, where P [V] is the magnitude of voltage pulse, I [A] is post−synaptic current, and t [s] is pulse width.[29] Post−synaptic current is linearly dependent on the device dimension, so the calculated energy consumption also has a linear dependency on the device dimension (**Figure 3.22**).[13] The magnitude of post−synaptic current was smallest in the 2D perovskite synapse; its calculated energy consumption was also lowest when voltage amplitude and pulse width were fixed. The calculated energy consumption of 2D perovskite synapse (~10 fJ per synaptic event for a device of 250 × 250 μm) is comparable to the energy consumed by biological synapses. If the size of the device can be reduced using state−of−art photolithography to (0.3 × 0.3 μm),[30,31] energy consumption can be reduced to ~0.026 aJ (**Figure 3.23**). Compared with the recently−reported energy consumption of fabricated artificial synapses (**Figure 3.23**, **Table 3.4**),[5,12,13,22,29,30,32–41] our perovskite synapses show much higher energy efficiency despite having larger dimension. This energy efficiency would be a great advantage in neuromorphic computing system.

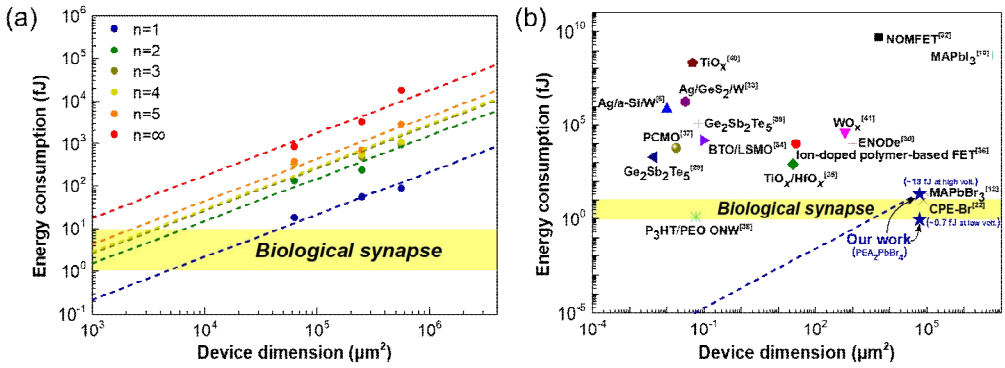

Figure 3.22 The energy consumption of our devices

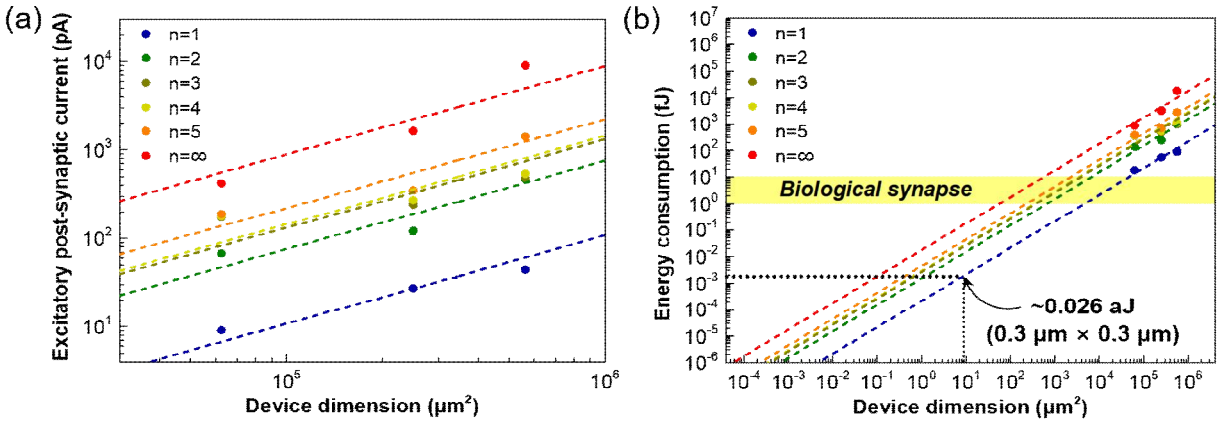

Figure 3.22 EPSC depending on the fabricated devices with dimension and energy consumption

Synaptic device	Dimensions	Energy consumption	Reference
NOMFET	5 × 1000 μm	~5 μJ	[32]
TiO_x	D = 250 nm	~200 nJ	[40]
$MAPbI_3$	6×10^{-2} cm^2	550 nJ	[13]
Ag/GeS_2 /W	D = 200 nm	1800-3100 pJ	[33]
Ag/a-Si/W	100 × 100 nm	~720 pJ	[5]
Ge_2 Sb_2 Te_5	D = 300 nm	121-1552 pJ	[39]
PCMO	D = 150 nm-1 μm	6-600 pJ	[37]
Ge_2 Sb_2 Te_5	D = 75 nm	2-50 pJ	[29]
BTO/LSMO	D = 350 nm	~15 pJ	[34]
WO_x	25 × 25 μm	~40 pJ	[41]
Ion-doped polymer-based FET	1.5 × 20 μm	10 pJ	[36]
ENODe	10^3 μm^3	~10 pJ	[30]
TiO_x /HfO_x	5 × 5 μm	0.85-24 pJ	[35]
PEO/P_3 HT Organic nano wire (ONW)	D = 100 nm	~1.23 fJ	[38]
Conjugated polyelectrolyte (CPE)-Br	8.02×10^{-4} cm^2	10-100 fJ	[22]
$MAPbBr_3$	8.02×10^{-4} cm^2	~20 fJ	[12]
$(PEA)_2$ $PbBr_4$	6.25×10^{-4} cm^2	~0.7 fJ	Our work

Table 3.4 Summary of device structures and energy consumption of artificial synaptic devices

Chapter 4. Conclusion

In conclusion, we reported halide perovskite artificial synapses that have energy consumption that is as low as that of a biological synapse. Artificial synapses composed of 2D, Quasi-2D, and 3D OHP films with various structural dimensionality emulated EPSC, PPF, STP, and LTP. The Quasi-2D OHP artificial synapse showed increased long-term memory retention over 3D OHP synapses, and had femtojoule-level energy consumption (18 fJ per synaptic event) which is similar to those of biological synapses (1-10 fJ per synaptic event). Energy consumption of the device can be further decreased to much lower than that of the biological synapse by using state-of-art photolithography to minimize the device size. We suggested an operation mechanism of perovskite artificial synapses by comparing the calculated activation energy for ion migration of perovskite films with different dimensionalities. We expect that our approach will have applications in perovskite artificial synapses to demonstrate energy-efficient neuromorphic computing.

Bibliography

[1] C. Eroglu, B. A. Barres, *Nature* 2010, *468*, 223.

[2] J. C. López, *Nat. Rev. Neurosci.* 2001, *2*, 148.

[3] P. A. Merolla, J. V. Arthur, R. Alvarez-Icaza, A. S. Cassidy, J. Sawada, F. Akopyan, B. L. Jackson, N. Imam, C. Guo, Y. Nakamura, B. Brezzo, I. Vo, S. K. Esser, R. Appuswamy, B. Taba, A. Amir, M. D. Flickner, W. P. Risk, R. Manohar, D. S. Modha, *Science* 2014, *345*, 668.

[4] D. Kuzum, R. G. D. Jeyasingh, B. Lee, H.-S. P. Wong, *Nano Lett.* 2012, *12*, 2179.

[5] S. H. Jo, T. Chang, I. Ebong, B. B. Bhadviya, P. Mazumder, W. Lu, *Nano Lett.* 2010, *10*, 1297.

[6] M. Gajek, J. J. Nowak, J. Z. Sun, P. L. Trouilloud, E. J. O' Sullivan, D. W. Abraham, M. C. Gaidis, G. Hu, S. Brown, Y. Zhu, R. P. Robertazzi, W. J. Gallagher, D. C. Worledge, *Appl. Phys. Lett.* 2012, *100*, 132408.

[7] T. Hasegawa, T. Ohno, K. Terabe, T. Tsuruoka, T. Nakayama, J. K. Cimzewski, M. Aono, *Adv. Mater.* 2010, *22*, 1831.

[8] Y. Lee, J. Y. Oh, W. Xu, O. Kim, T. R. Kim, J. Kang, Y. Kim, D. Son, J. B.-H. Tok, M. J. Park, Z. Bao, T.-W. Lee, *Sci. Adv.* 2018, *4*, eaat7387.

[9] Y. Kim, A. Chortos, W. Xu, Y. Liu, J. Y. Oh, D. Son, J. Kang, A. M. Foudeh, C. Zhu, Y. Lee, S. Niu, J. Liu, R. Pfattner, Z. Bao, T.-W. Lee, *Science (80-.).* 2018, *360*, 998.

[10] Y.-H. Kim, H. Cho, T.-W. Lee, *Proc. Natl. Acad. Sci.* 2016, *113*, 11694.

[11] J. M. Frost, K. T. Butler, F. Brivio, C. H. Hendon, M. Van

Schilfgaarde, A. Walsh, *Nano Lett.* 2014, *14*, 2584.

[12] W. Xu, H. Cho, Y.-H. Kim, Y.-T. Kim, C. Wolf, C.-G. Park, T.-W. Lee, *Adv. Mater.* 2016, *28*, 5916.

[13] Z. Xiao, J. Huang, *Adv. Electron. Mater.* 2016, *2*, 1600100.

[14] J. Byun, H. Cho, C. Wolf, M. Jang, A. Sadhanala, R. H. Friend, H. Yang, T.-W. Lee, *Adv. Mater.* 2016, *28*, 7515.

[15] X. Xiao, J. Dai, Y. Fang, J. Zhao, X. Zheng, S. Tang, P. N. Rudd, X. C. Zeng, J. Huang, *ACS Energy Lett.* 2018, *3*, 684.

[16] J. Y. Seo, J. Choi, H. S. Kim, J. Kim, J. M. Yang, C. Cuhadar, J. S. Han, S. J. Kim, D. Lee, H. W. Jang, N. G. Park, *Nanoscale* 2017, *9*, 15278.

[17] K. Tanaka, T. Kondo, *Sci. Technol. Adv. Mater.* 2003, *4*, 599.

[18] L. Dou, A. B. Wong, Y. Yu, M. Lai, N. Kornienko, S. W. Eaton, A. Fu, C. G. Bischak, J. Ma, T. Ding, N. S. Ginsberg, L.-W. Wang, A. P. Alivisatos, P. Yang, *Science* 2015, *349*, 1518.

[19] L.-C. Chen, Z.-L. Tseng, J.-K. Huang, C.-C. Chen, S. Chang, *Coatings* 2016, *6*, 53.

[20] T. Chang, S. H. Jo, W. Lu, *ACS Nano* 2011, *5*, 7669.

[21] L. F. Abbott, W. G. Regehr, *Nature* 2004, *431*, 796.

[22] W. Xu, T. L. Nguyen, Y. T. Kim, C. Wolf, R. Pfattner, J. Lopez, B. G. Chae, S. Il Kim, M. Y. Lee, E. Y. Shin, Y. Y. Noh, J. H. Oh, H. Hwang, C. G. Park, H. Y. Woo, T. W. Lee, *Nano Energy* 2018, *48*, 575.

[23] T. Ohno, T. Hasegawa, T. Tsuruoka, K. Terabe, J. K. Gimzewski, M. Aono, *Nat. Mater.* 2011, *10*, 591.

[24] L. Malavasi, C. A. J. Fisher, M. S. Islam, *Chem. Soc. Rev.* 2010, *39*, 4370.

[25] Y. Chen, Y. Sun, J. Peng, J. Tang, K. Zheng, Z. Liang, *Adv. Mater.* 2018, *30*, 1.

[26] J. M. Azpiroz, E. Mosconi, J. Bisquert, F. De Angelis, *Energy Environ. Sci.* 2015, *8*, 2118.

[27] C. Eames, J. M. Frost, P. R. F. Barnes, B. C. O' Regan, A. Walsh, M. S. Islam, *Nat. Commun.* 2015, *6*, 2.

[28] S. Meloni, T. Moehl, W. Tress, M. Franckevičius, M. Saliba, Y. H. Lee, P. Gao, M. K. Nazeeruddin, S. M. Zakeeruddin, U. Rothlisberger, M. Graetzel, *Nat. Commun.* 2016, *7*, 10334.

[29] D. Kuzum, S. Yu, H.-S. Philip Wong, *Nanotechnology* 2013, *24*, 382001.

[30] Y. van de Burgt, E. Lubberman, E. J. Fuller, S. T. Keene, G. C. Faria, S. Agarwal, M. J. Marinella, A. Alec Talin, A. Salleo, *Nat. Mater.* 2017, *16*, 414.

[31] Y. Zhang, J. R. Petta, S. Ambily, Y. Shen, D. C. Ralph, G. G. Malliaras, *Adv. Mater.* 2003, *15*, 1632.

[32] F. Alibart, S. Pleutin, O. Bichler, C. Gamrat, T. Serrano-Gotarredona, B. Linares-Barranco, D. Vuillaume, *Adv. Funct. Mater.* 2012, *22*, 609.

[33] M. Suri, O. Bichler, D. Querlioz, G. Palma, E. Vianello, D. Vuillaume, C. Gamrat, B. DeSalvo, in *2012 Int. Electron Devices Meet.*, IEEE, 2012, p. 10.3.1-10.3.4.

[34] A. Chanthbouala, A. Crassous, V. Garcia, K. Bouzehouane, S. Fusil, X. Moya, J. Allibe, B. Dlubak, J. Grollier, S. Xavier, C. Deranlot, A. Moshar, R. Proksch, N. D. Mathur, M. Bibes, A. Barthélémy, *Nat. Nanotechnol.* 2012, *7*, 101.

[35] S. Yu, B. Gao, Z. Fang, H. Yu, J. Kang, H.-S. P. Wong, in *2012 Int. Electron Devices Meet.*, IEEE, 2012, p. 10.4.1-10.4.4.

[36] Q. Lai, L. Zhang, Z. Li, W. F. Stickle, R. S. Williams, Y. Chen, *Appl. Phys. Lett.* 2009, *95*, 213503.

[37] S. Park, M. Chu, J. Kim, J. Noh, M. Jeon, B. Hun Lee, H.

Hwang, B. Lee, B. Lee, *Sci. Rep.* 2015, *5*, 10123.

[38] W. Xu, S. Min, H. Hwang, T. Lee, *Sci. Adv.* 2016, *2*, e1501326.

[39] M. Suri, O. Bichler, D. Querlioz, B. Traoré, O. Cueto, L. Perniola, V. Sousa, D. Vuillaume, C. Gamrat, B. DeSalvo, *J. Appl. Phys.* 2012, *112*, 054904.

[40] K. Seo, I. Kim, S. Jung, M. Jo, S. Park, J. Park, J. Shin, K. P. Biju, J. Kong, K. Lee, B. Lee, H. Hwang, *Nanotechnology* 2011, *22*, 254023.

[41] R. Yang, K. Terabe, G. Liu, T. Tsuruoka, T. Hasegawa, J. K. Gimzewski, M. Aono, *ACS Nano* 2012, *6*, 9515.

Abstract

유기/무기 하이브리드 페로브스카이트 재료는 이온 이동에 의해 유발되는 특수한 히스테리시스 성질을 기반으로 한 인공 시냅스의 활성 물질로서 각광받고 있는 재료이다. 이전에 보고된 3 차원 페로브스카이트 인공 시냅스 소자가 생물학적 시냅스의 시냅스 가소성을 성공적으로 모사하였지만, 소자의 메모리 유지시간과 에너지 소모는 아직 더 해결해야 할 과제이다. 여기서 우리는 2 차원과 준 2 차원 페로브스카이트 재료를 사용하여, 2 단자 인공시냅스를 구현하였는데, 2 차원과 준 2 차원 페로브스카이트 재료는 메틸암모늄 브로마이드 구조에서 주기적인 절연체인 펜에틸암모늄 층이 섞여있는 구조를 갖고 있다. 다양한 차원에 따라서 페로브스카이트 박막의 광학적 특성과 형상을 확인하여 비교를 하였으며, 이러한 박막으로 만들어낸 소자의 시냅스 특성 (단기가소성, 장기가소성) 도 분석하여 비교를 하였다. 또한, 준 2 차원 페로브스카이트 인공 시냅스 소자의 작동 메커니즘을 3 차원 페로브스카이트 인공 시냅스 소자와 비교하여 분석하였는데, 이온 이동을 위한 활성화 에너지의 크기를 비교함으로써 메모리 유지시간이 증진되는 것을 확인할 수 있었다. 또한, 준 2 차원 페로브스카이트 인공 시냅스 소자가 소모하는 에너지 (18 fJ/시냅스 사건) 가 생물학적 시냅스가 소모하는 에너지의 크기(1-10 fJ/시냅스 사건)와 근접한 수준이었다. 이 연구가 페로브스카이트 인공 시냅스를 기반으로 한 저에너지 뉴로모픽 일렉트로닉스를 가능하게 할 것이다.

주요어 : 뉴로모픽 메모리, 페로브스카이트 멤리스터, 인공시냅스, 준 2D 페로브스카이트, 페로브스카이트 시냅스

학 번 : 2017-21688